Institute of High Energy Physics
Chinese Academy of Sciences

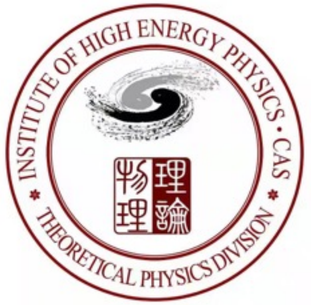

Pulsar Polarization Arrays

Jing Ren (任婧)

Theoretical Physics Division, IHEP

IAS Program on High Energy Physics (mini-workshop: theory)

Jan. 13, 2022

Based on work with Tao Liu, Xuzixiang Lou, arXiv: 2111.10615

Content

- Pulsar timing arrays (PTAs) and pulsar polarization arrays (PPAs)
- Ultralight axion-like dark matter (ALDM)
- Ultralight scalar DM detection by PTAs
- ALDM detection by PPAs through cosmic birefringence

Pulsars

- Pulsars emit electromagnetic pulses with extraordinary regularity, with the period ranging from milliseconds to seconds. Up to now about 3000 pulsars observed in our galaxy
- Millisecond pulsars (MSPs) are especially stable due to mass and angular momentum transfer from a companion. Although emission mechanism not fully clarified, they play significant roles as astronomical clocks

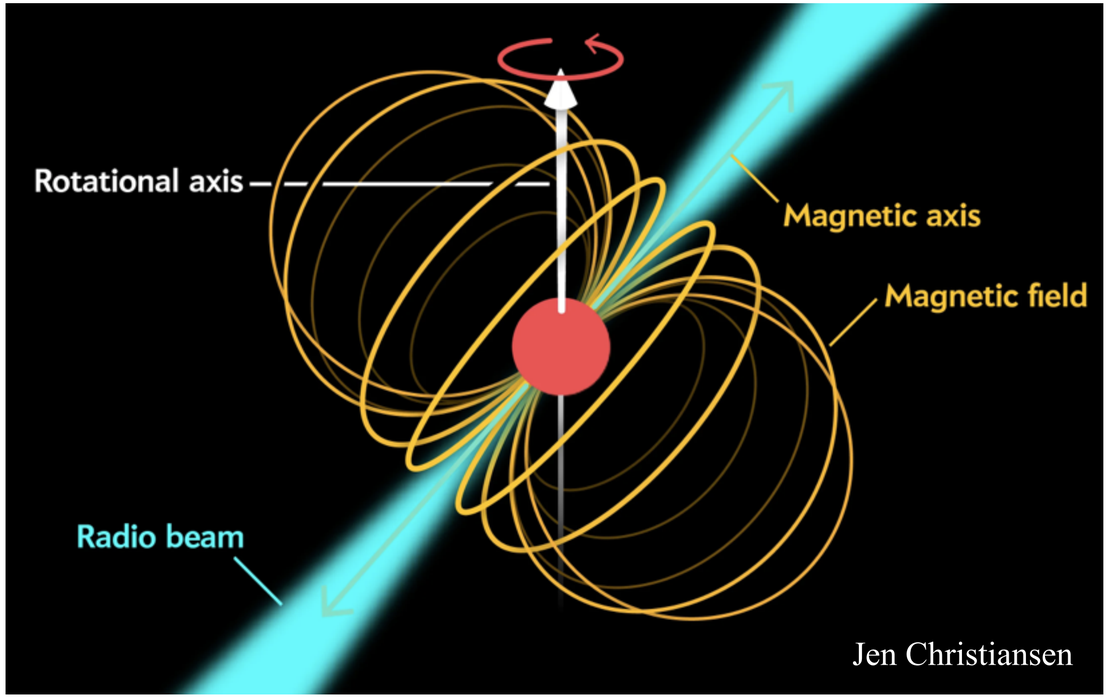

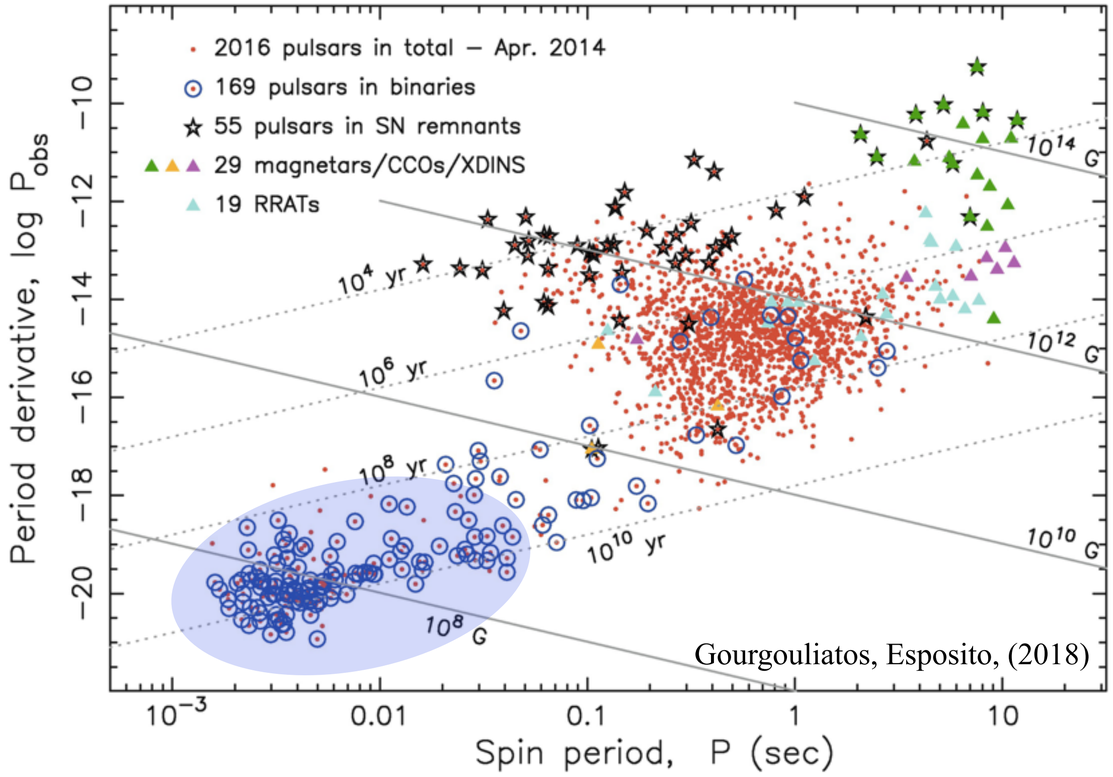

Pulsar timing arrays (PTAs)

- Over 80 MSPs are monitored by the global PTA network in the timespan of years. Future radio telescopes (FAST/SKA) may increase the number to the order of 1000.

- Given precise timing model of the expected time of arrival of the pulse, the measured **time difference** can be directly related to **gravitational waves (GWs)**

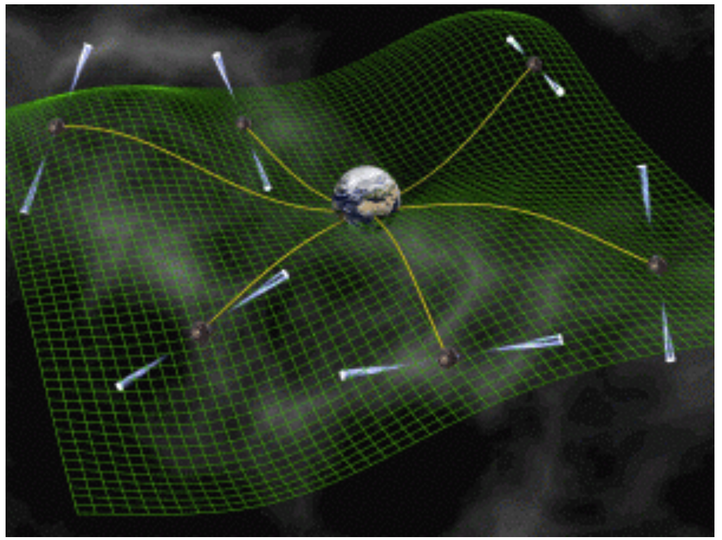

$$\Delta T(t) = \int_{-\infty}^{\infty} df \frac{1}{2} u^a u^b h_{ab}(f,\hat{n})\, e^{i2\pi f(t+\hat{n}\cdot\vec{r}_2/c)} \frac{1}{i2\pi f} \frac{1}{1+\hat{n}\cdot\hat{u}} \left[1 - e^{-\frac{i2\pi f L}{c}(1+\hat{n}\cdot\hat{u})}\right]$$

metric perturbation "Earth" "pulsar"

Pulsar timing arrays (PTAs)

- Over 80 MSPs are monitored by the global PTA network in the timespan of years. Future radio telescopes (FAST/SKA) may increase the number to the order of 1000.

- Given precise timing model of the expected time of arrival of the pulse, the measured **time difference** can be directly related to **gravitational waves (GWs)**

$$\Delta T(t) = \int_{-\infty}^{\infty} df \frac{1}{2} u^a u^b h_{ab}(f,\hat{n})\, e^{i2\pi f(t+\hat{n}\cdot\vec{r}_2/c)} \frac{1}{i2\pi f} \frac{1}{1+\hat{n}\cdot\hat{u}} \left[1 - e^{-\frac{i2\pi f L}{c}(1+\hat{n}\cdot\hat{u})}\right]$$

metric perturbation — "Earth" — "pulsar"

- PTAs serve as galactic interferometers to measure nHZ GWs. With MSPs in different directions, stochastic GW backgrounds (SGWBs) can be identified by the quadrupolar spatial correlations among pulsars

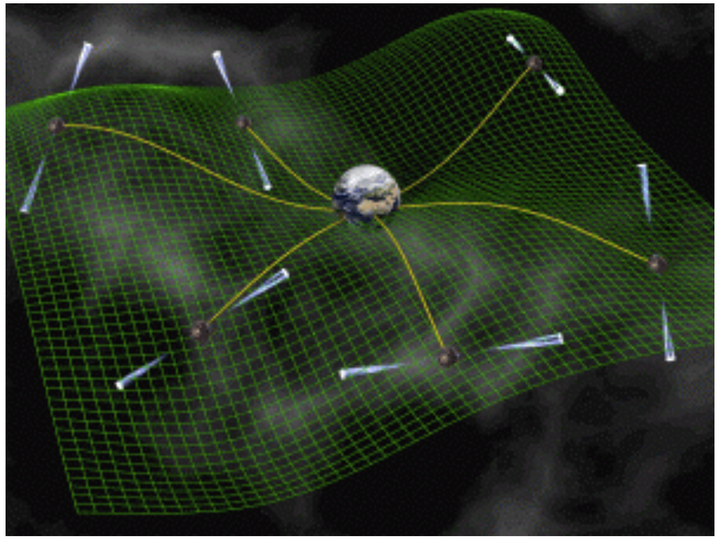

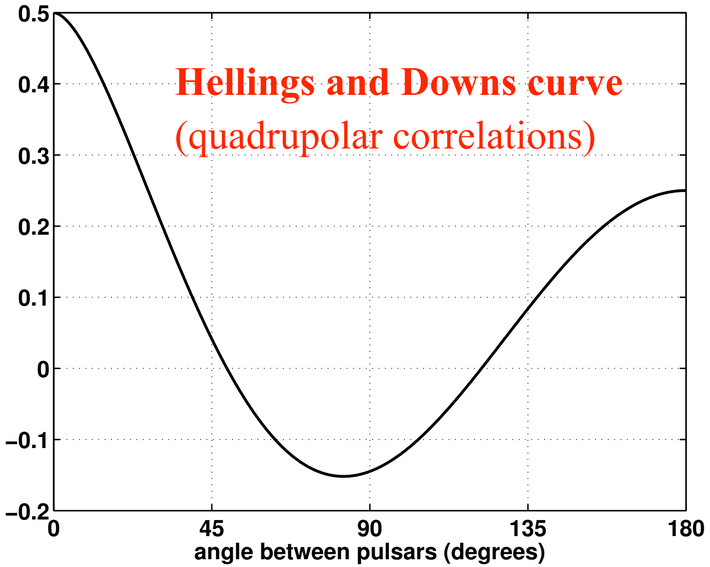

Pulsar timing arrays (PTAs)

Recently, the explorations on the PTA targets extended to dark matter (DM) physics

Oscillating gravitational potential induced by ultralight scalar DM

Khmelnitsky and Rubakov, 1309.5888; De Martino et al. 1705.04367; Porayko et al., 1810.03227

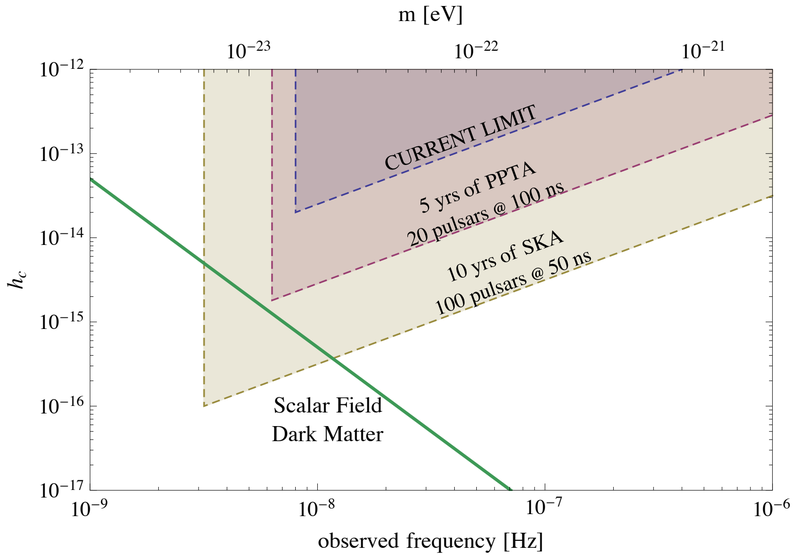

more details latter…

Doppler/Shapiro effects induced by transiting objects associated with DM substructure

Zurek and collaborators, 1901.04490, 2005.03030, 2104.05717

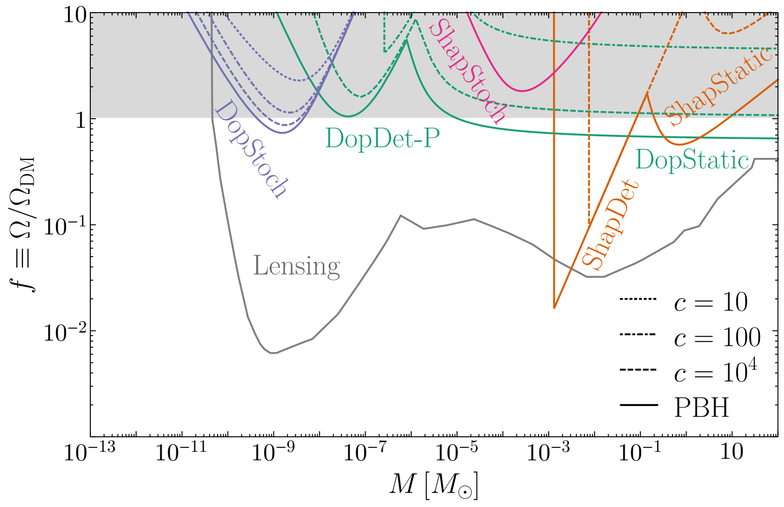

Oscillating fifth force induced by ultralight dark photon DM

Xue et al. [PPTA], 2112.07687

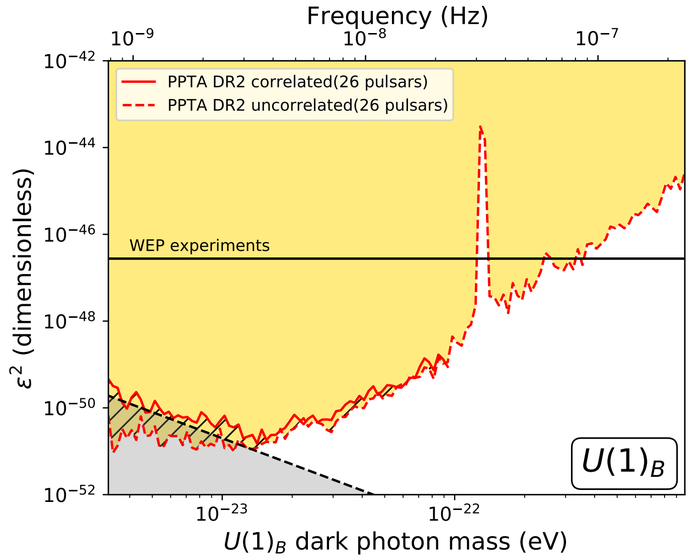

see Qiang Yuan's talk

Pulsar polarization arrays (PPAs)

- Pulsars radio emissions typically have strong linear polarization

#	NAME		P0 (s)			DM (cm^-3 pc)			RM (rad m^-2)			DIST (kpc)
1	J0002+6216	cwp+17	0.1153635682680	14	cwp+17	218.6	6	wcp+18	*	0	*	6.357
2	J0006+1834	cnt96	0.69374767047	14	cn95	11.41	55	bkk+16	-20	3	npn+20	0.860
3	J0007+7303	aaa+09c	0.3158731909	3	awd+12	*	0	*	*	0	*	1.400
4	J0011+08	dsm+16	2.55287	0	dsm+16	24.9	0	dsm+16	*	0	*	5.399
5	B0011+47	dth78	1.240699038946	11	hlk+04	30.405	13	bkk+16	-15.56	10	sbg+19	1.776
36	J0026+6320	jml+09	0.31835777079	3	sjm+19	245.06	6	sjm+19	-294	2	npn+20	6.619
37	J0030+0451	lzb+00	0.0048654532114961	19	aab+21a	4.332772	0	aab+21a	1.17	8	sbg+19	0.324
38	J0033+57	hrk+08	0.315	0	hrk+08	75.65	9	mss+20	*	0	*	2.251
39	J0033+61	hrk+08	0.912	0	hrk+08	37.7	3	mss+20	*	0	*	1.654
40	J0034-0534	bhl+94	0.0018771818845850	2	aaa+10b	13.76517	4	aaa+10b	-38	17	hmvd18	1.348
96	B0144+59	stwd85	0.19632137543003	16	ywml10	40.111	3	hlk+04	-9.5	5	npn+20	2.128
97	B0148-06	mlt+78	1.464664549334	7	hlk+04	25.66	3	hlk+04	2	4	hl87	25.000
98	J0152+0948	clm+05	2.74664729014	10	clm+05	22.881	12	bkk+16	1.4	2	sbg+19	2.477
99	B0149-16	mlt+78	0.8327416126878	13	hlk+04	11.92577	4	srb+15	+6.6	50	fdr15	0.920
100	J0154+1833	mgf+19	0.0023645697763006	5	mgf+19	19.7978	1	mgf+19	21.6	1	mgf+19	1.622
366	J0818-3232	bjd+06	2.161258926939	15	bjd+06	131.80	7	bjd+06	25.2	50	hmvd18	0.484
367	B0818-13	vl70	1.2381295438682	8	hlk+04	40.938	3	hlk+04	-1.2	4	hl87	1.900
368	J0820-3826	bkl+13	0.1248366735581	5	psj+19	195.50	3	mss+20	+122	6	jsd+21	4.084
369	J0820-3921	bjd+06	1.07356658405	4	bjd+06	179.4	1	bjd+06	126.9	71	hmvd18	3.576
370	B0818-41	mlt+78	0.5454455601	3	lbs+20	113.4	2	antt94	57.7	5	qmlg95	0.571

ATNF Pulsar Catalogue
(Version: 1.66)

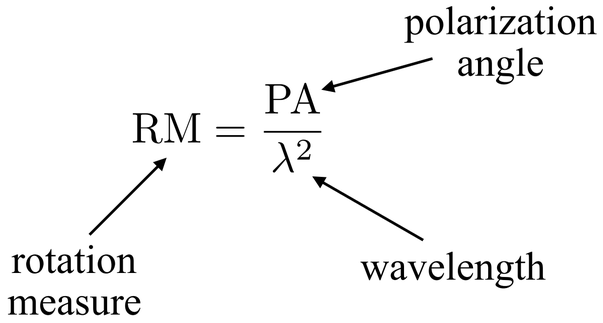

- For precise timing, polarization calibration plays a crucial role, and polarization profiles are usually obtained as a by-product

Pulsar polarization arrays (PPAs)

- Pulsars radio emissions typically have strong linear polarization

#	NAME		P0 (s)			DM (cm^-3 pc)			RM (rad m^-2)			DIST (kpc)
1	J0002+6216	cwp+17	0.1153635682680	14	cwp+17	218.6	6	wcp+18	*	0	*	6.357
2	J0006+1834	cnt96	0.69374767047	14	cn95	11.41	55	bkk+16	-20	3	npn+20	0.860
3	J0007+7303	aaa+09c	0.3158731909	3	awd+12	*	0	*	*	0	*	1.400
4	J0011+08	dsm+16	2.55287	0	dsm+16	24.9	0	dsm+16	*	0	*	5.399
5	B0011+47	dth78	1.240699038946	11	hlk+04	30.405	13	bkk+16	-15.56	10	sbg+19	1.776
36	J0026+6320	jml+09	0.31835777079	3	sjm+19	245.06	6	sjm+19	-294	2	npn+20	6.619
37	J0030+0451	lzb+00	0.0048654532114961	19	aab+21a	4.332772	0	aab+21a	1.17	8	sbg+19	0.324
38	J0033+57	hrk+08	0.315	0	hrk+08	75.65	9	mss+20	*	0	*	2.251
39	J0033+61	hrk+08	0.912	0	hrk+08	37.7	3	mss+20	*	0	*	1.654
40	J0034-0534	bhl+94	0.0018771818845850	2	aaa+10b	13.76517	4	aaa+10b	-38	17	hmvd18	1.348
96	B0144+59	stwd85	0.19632137543003	16	ywml10	40.111	3	hlk+04	-9.5	5	npn+20	2.128
97	B0148-06	mlt+78	1.464664549334	7	hlk+04	25.66	3	hlk+04	2	4	hl87	25.000
98	J0152+0948	clm+05	2.74664729014	10	clm+05	22.881	12	bkk+16	1.4	2	sbg+19	2.477
99	B0149-16	mlt+78	0.8327416126878	13	hlk+04	11.92577	4	srb+15	+6.6	50	fdr15	0.920
100	J0154+1833	mgf+19	0.0023645697763006	5	mgf+19	19.7978	1	mgf+19	21.6	1	mgf+19	1.622
366	J0818-3232	bjd+06	2.161258926939	15	bjd+06	131.80	7	bjd+06	25.2	50	hmvd18	0.484
367	B0818-13	vl70	1.2381295438682	8	hlk+04	40.938	3	hlk+04	-1.2	4	hl87	1.900
368	J0820-3826	bkl+13	0.1248366735581	5	psj+19	195.50	3	mss+20	+122	6	jsd+21	4.084
369	J0820-3921	bjd+06	1.07356658405	4	bjd+06	179.4	1	bjd+06	126.9	71	hmvd18	3.576
370	B0818-41	mlt+78	0.5454455601	3	lbs+20	113.4	2	antt94	57.7	5	qmlg95	0.571

ATNF Pulsar Catalogue
(Version: 1.66)

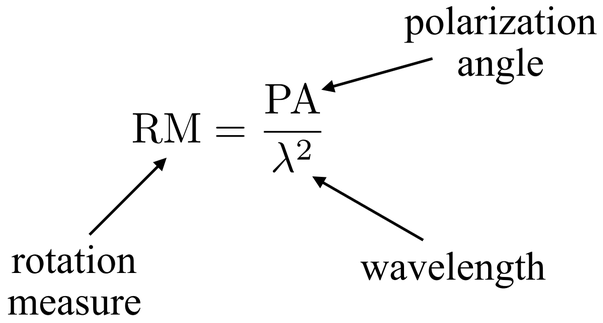

- For precise timing, polarization calibration plays a crucial role, and polarization profiles are usually obtained as a by-product

- With the same data acquired for PTAs, we propose the development of PPAs in addition to explore more in astrophysics and fundamental physics. Extend the potential physical reach of radio telescope resources

Pulsar polarization arrays (PPAs)

- Measured polarization angle

$$\mathrm{PA} = \mathrm{PA}_{\mathrm{source}} + \mathrm{PA}_{\mathrm{instr}} + \mathrm{PA}_{\mathrm{noise}} + \mathrm{PA}_{\mathrm{jitter}} + \mathrm{PA}_{\mathrm{FR}} + \mathrm{PA}_{\mathrm{NP}}$$

  - "source": variations due to changes in pulsar orientation or its magnetosphere
  - "instr": related to PA calibration (conversion of measured PA to absolute one)
  - "noise": the radiometer noise (inversely proportional to SNR)
  - "jitter": jitter noise unique to pulsars due to stochastic variation of single pulse profile
  - "FR": Faraday rotation caused by interstellar magnetic field as well as Earth's ionosphere
  - "NP": new physics contribution…

- As in the case of PTAs, with widely distributed MSPs, PPAs are best suited to reveal **temporal and spatial correlations at large scales**, difficult to be mimicked by other sources

Axion and axion-like particles (ALPs)

- QCD axion well motivated to solve the strong CP problem, where m_a and f_a relation fixed, and also serve as an DM candidate
- ALPs (light pseudo-Goldstone bosons) introduced in many BSM scenarios, e.g. string axions. m_a and f_a can vary more freely in a wider range
- Ultralight ALPs (m_a<10^{-18}eV) can be generated as a Bose-Einstein condensate from misalignment; behave effectively as a classical scalar field
- Ultralight ALPs may serve as DM or DE during cosmic evolution. In this talk, we focus on ALDM (e.g. fuzzy DM at m_a~10^{-22}eV, subdominant at m_a<10^{-24}eV)

ALPs landscapes

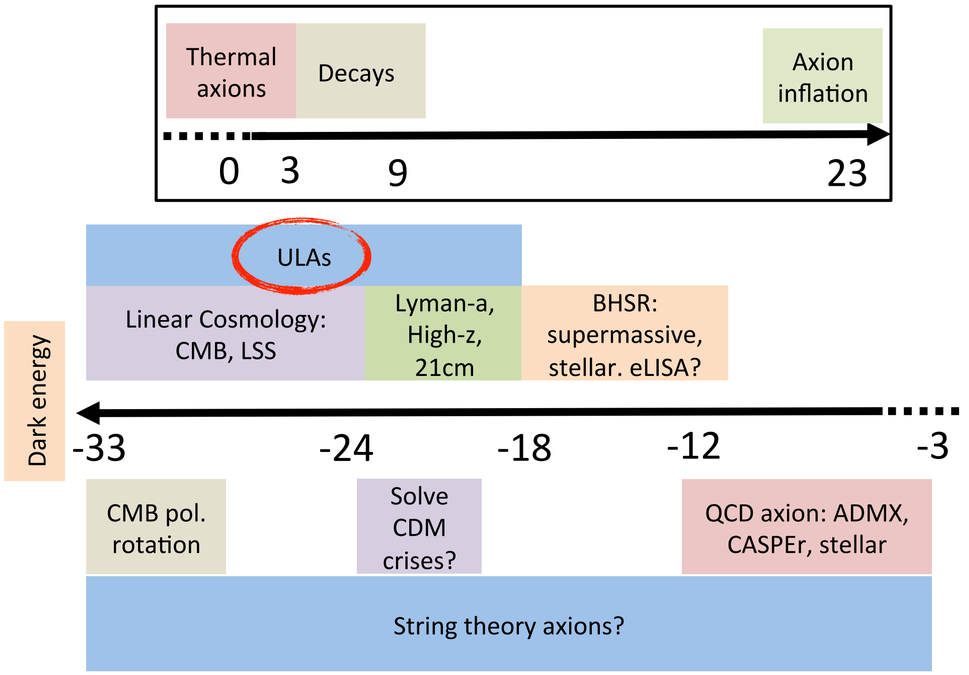

$\log_{10}(m_a/\mathrm{eV})$

D. Marsh, Phys. Rept. 643, 1-79 (2016)

Physical properties of ALDM

- Local ALDM field with density $\rho(\mathbf{x})$ made up by a large number of ALPs, i.e. classical fields with uncorrelated random phases Foster, Rodd, Safdi, PRD 97, no.12, 123006 (2018)

$$a(\mathbf{x},t) \;\approx\; \frac{\sqrt{\rho(\mathbf{x})}}{m_a}\int \alpha_{\mathbf{v}}\sqrt{f_{\mathbf{x}}(\mathbf{v})}\,\cos[\omega_a(t-\mathbf{v}\cdot\mathbf{x})+\phi_{\mathbf{v}}]\,d^3\mathbf{v}\,.$$

  - Non-relativistic limit: $\omega_a \approx m_a,\ \mathbf{k}\approx m_a\mathbf{v}$; velocity distribution $f_{\mathbf{x}}(\mathbf{v})$ peaked around $|\mathbf{v}|\sim v_0\sim 10^{-3}c$ (CDM velocity in our galaxy)
  - Random nature of ALPs captured by random amplitude $\alpha_{\mathbf{v}}$ and phase $\phi_{\mathbf{v}}$ (follow the Rayleigh and uniform distributions)

- ALPs effective action: gravitational interaction, coupling to SM particles…

$$S=\int d^4x\sqrt{-g}\left[\frac{1}{2}\nabla^\mu a\nabla_\mu a-\frac{1}{2}m_a^2a^2+\frac{g_{a\gamma}}{2}aF_{\mu\nu}\tilde{F}^{\mu\nu}+\frac{g_{af}}{2m_f}\nabla_\mu a(\bar{f}\gamma^\mu\gamma_5 f)+\ldots\right]$$

Chern-Simons coupling spin-dependent

Ultralight scalar DM induced oscillation

Khmelnitsky and Rubakov, JCAP 02, 019 (2014)

Energy-momentum tensor of a free scalar field ϕ in non-relativistic limit:

$$T_{00} = \frac{1}{2}m^2A^2 \equiv \rho_{DM}\,, \quad T_{ij} = -\frac{1}{2}m^2A^2\cos(\omega t + 2\alpha)\,\delta_{ij} \equiv p(\mathbf{x},t)\,\delta_{ij}\,, \quad \omega = 2m \quad \text{(average } p \text{ equal to zero)}$$

Gravitational potential split into two parts: $\Psi(\mathbf{x},t) \simeq \Psi_0(\mathbf{x}) + \Psi_c(\mathbf{x})\cos(\omega t + 2\alpha(\mathbf{x})) + \Psi_s(\mathbf{x})\sin(\omega t + 2\alpha(\mathbf{x}))$

- Time-independent part determined by Einstein equation 00 component (Poisson equation)

$$\Delta\Psi = 4\pi G T_{00} = 4\pi G\rho_{DM} \longrightarrow \Psi_0 \sim G\rho_{DM}/k^2$$

- Oscillating part determined by Einstein equation ij component

$$-6\ddot{\Psi} + 2\Delta(\Psi - \Phi) = 8\pi G\,T_{kk} = 24\pi G\,p(\mathbf{x},t) \longrightarrow \Psi_c(\mathbf{x}) = \frac{1}{2}\pi G A(\mathbf{x})^2 = \pi\frac{G\rho_{DM}(\mathbf{x})}{m^2}$$

oscillating part Ψ_c is $(k/m)^2 \sim v_0^2$ times smaller than time-independent part Ψ_0

Effect on pulsar timing

Oscillating gravitational potential changes the arrival frequency and time of the pulse,

$$\frac{\Omega(t)-\Omega_0}{\Omega_0} = \Psi(\mathbf{x},t) - \Psi(\mathbf{x}_\mathbf{p},t') - \int_{t'}^{t} n_i \partial_i \big(\Psi(\mathbf{x}'',t'') + \Phi(\mathbf{x}'',t'')\big)\, dt''$$

(suppressed by $|\mathbf{k}|/\omega \sim 10^{-3}$)

As for GW, the induced timing residual also has "Earth" and "pulsar" terms

$$\Delta t(t) = -\int_0^t \frac{\Omega(t')-\Omega_0}{\Omega_0}\, dt' = \frac{\Psi_c(x_e)}{2\pi f}\sin[2\pi f t + 2\alpha(x_e)] - \frac{\Psi_c(x_p)}{2\pi f}\sin\left[2\pi f\left(t-\frac{d_p}{c}\right)+2\alpha(x_p)\right]$$

$$f = \frac{2m}{2\pi} = 4.8\times10^{-8}\left(\frac{m}{10^{-22}\mathrm{eV}}\right)\mathrm{Hz}\,,\ \Psi_c = \frac{G\rho_{\mathrm{SF}}}{\pi f^2} \approx 6.1\times10^{-18}\left(\frac{m}{10^{-22}\,\mathrm{eV}}\right)^{-2}\left(\frac{\rho_{\mathrm{SF}}}{0.4\,\mathrm{GeV\,cm^{-3}}}\right)$$

Considering pulsars close-by, $\Psi_c(x_e) \approx \Psi_c(x_p)$, ultralight scalar DM induced oscillation is similar to that induced by monochromatic GW backgrounds with characteristic strain: $h_c = 2\sqrt{3}\,\Psi_c$

$$\Delta t_{GW} = \frac{h_c}{\omega}\sin\left(\frac{\omega D(1-\cos\theta)}{2}\right)(1+\cos\theta)\sin(2\psi)$$

Upper limits from PTAs

- Induced timing residual amplitude larger at lower mass: >20ns for $m<10^{-23}$ eV

$$\delta t \approx 0.02\,\mathrm{ns}\left(\frac{m}{10^{-22}\,\mathrm{eV}}\right)^{-3}\left(\frac{\rho_{\mathrm{SF}}}{0.4\,\mathrm{GeV\ cm^{-3}}}\right)$$

- Upper limits from current PPTA (25 MSPs, two week cadence) too weak to constrain ultralight scalar DM; forecasted limits improved with lower noise, more pulsars, more data points…

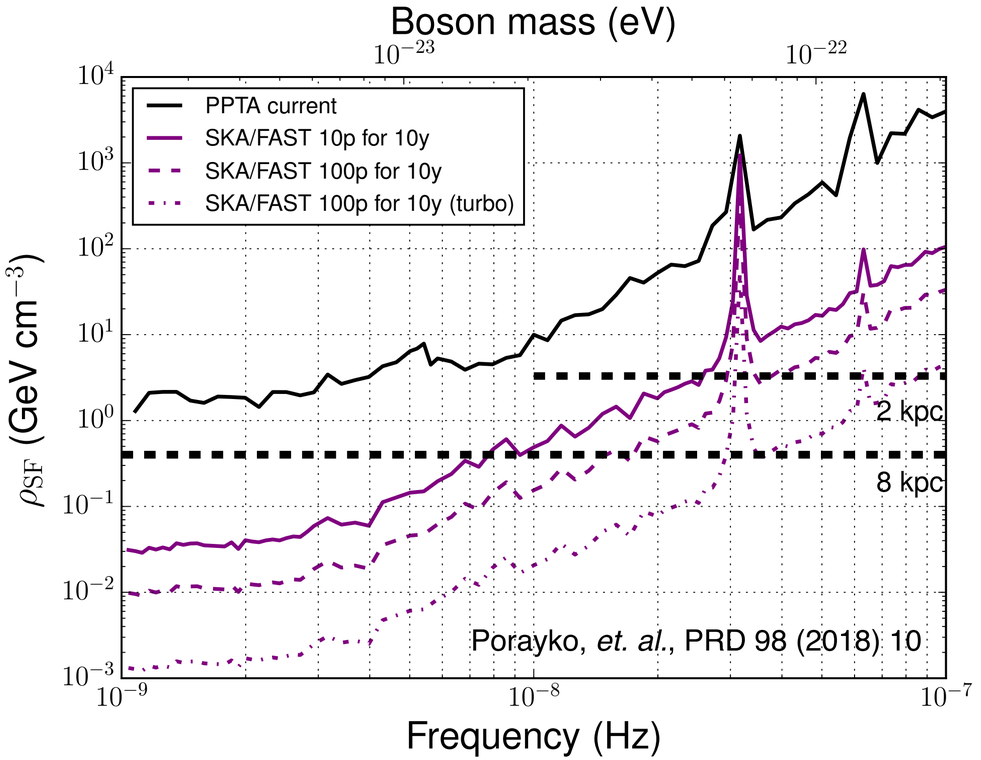

Upper limits from PTAs

- Induced timing residual amplitude larger at lower mass: >20ns for m<10^{-23}eV

$$\delta t \approx 0.02\,\mathrm{ns}\left(\frac{m}{10^{-22}\,\mathrm{eV}}\right)^{-3}\left(\frac{\rho_{\mathrm{SF}}}{0.4\,\mathrm{GeV\ cm^{-3}}}\right)$$

- Upper limits from current PPTA (25 MSPs, two week cadence) too weak to constrain ultralight scalar DM; forecasted limits improved with lower noise, more pulsars, more data points…

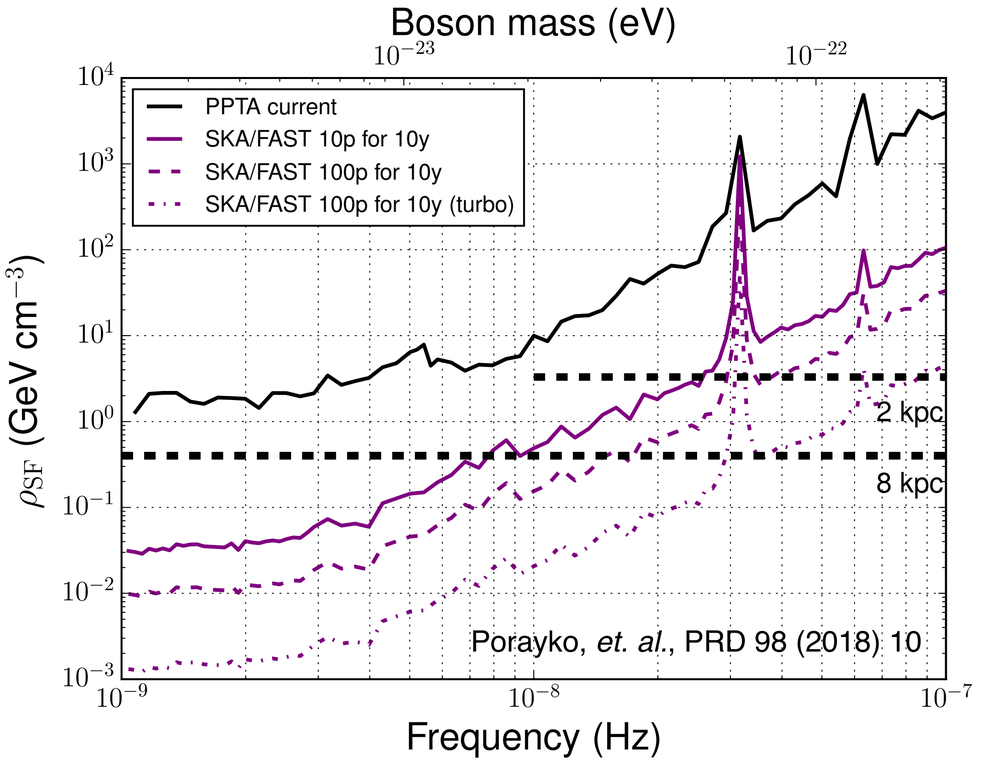

- Two caveats
  - Only consider MSPs nearby. Sensitivity greatly improved for MSPs within galactic bulge or near galactic center due to the much larger DM density De Martino et.al,, PRL 119, no.22, 221103 (2017)
  - Sensitivity mainly from oscillation in time; spatial-correlation not taken into account

ALDM induced cosmic birefringence

While photons propagate in ALDM field a, the Chern-Simons coupling to photon ($\frac{1}{2}gaF_{\mu\nu}\tilde{F}^{\mu\nu}$) corrects the dispersion relations of their two circular polarization modes

$$\omega_{\pm} \simeq k \pm g\left(\frac{\partial a}{\partial t} + \nabla a \cdot \frac{\mathbf{k}}{k}\right) \xrightarrow[\text{relativistic}]{\text{non}-} k \pm g\frac{\partial a}{\partial t}$$

For linearly polarized photons, this yields polarization angle (PA) rotation

$$\Delta\theta_{p,n} = \frac{g}{m_a}\int \alpha_{\mathbf{v}}\left\{\sqrt{\rho_p f_p(\mathbf{v})}\cos[m_a(t_n - L_p - \mathbf{v}\cdot\mathbf{x}_p) + \phi_{\mathbf{v}}] - \sqrt{\rho_e f_e(\mathbf{v})}\cos\left(m_a t_n + \phi_{\mathbf{v}}\right)\right\} d^3\mathbf{v}$$

(p denotes light source: $L_{\rm p}$ is distance to Earth; $t_{\rm n}$ is signal receiving time; others for ALDM field properties)

ALDM induced cosmic birefringence

While photons propagate in ALDM field a, the Chern-Simons coupling to photon ($\frac{1}{2}gaF_{\mu\nu}\tilde{F}^{\mu\nu}$) corrects the dispersion relations of their two circular polarization modes

$$\omega_{\pm} \simeq k \pm g\left(\frac{\partial a}{\partial t} + \nabla a \cdot \frac{\mathbf{k}}{k}\right) \xrightarrow[\text{relativistic}]{\text{non}-} k \pm g\frac{\partial a}{\partial t}$$

For linearly polarized photons, this yields polarization angle (PA) rotation

$$\Delta\theta_{p,n} = \frac{g}{m_a}\int \alpha_{\mathbf{v}}\left\{\sqrt{\rho_p f_p(\mathbf{v})}\cos[m_a(t_n - L_p - \mathbf{v}\cdot\mathbf{x}_p) + \phi_{\mathbf{v}}] - \sqrt{\rho_e f_e(\mathbf{v})}\cos\left(m_a t_n + \phi_{\mathbf{v}}\right)\right\} d^3\mathbf{v}$$

(p denotes light source: L_p is distance to Earth; t_n is signal receiving time; others for ALDM field properties)

Difference from Faraday rotation by galactic magnetic field

- relies only on field profiles at two endpoints of photon traveling (i.e. the "Earth" and "pulsar" terms)
- quasi-monochromatic oscillation around the frequency $\omega_a \approx m_a$
- no radio frequency dependence (FR increases with wavelength)

ALDM induced cosmic birefringence

While photons propagate in ALDM field a, the Chern-Simons coupling to photon ($\frac{1}{2}gaF_{\mu\nu}\tilde{F}^{\mu\nu}$) corrects the dispersion relations of their two circular polarization modes

$$\omega_{\pm} \simeq k \pm g\left(\frac{\partial a}{\partial t} + \nabla a \cdot \frac{\mathbf{k}}{k}\right) \xrightarrow[\text{relativistic}]{\text{non}-} k \pm g\frac{\partial a}{\partial t}$$

For linearly polarized photons, this yields polarization angle (PA) rotation

$$\Delta\theta_{p,n} = \frac{g}{m_a}\int \alpha_{\mathbf{v}}\left\{\sqrt{\rho_p f_p(\mathbf{v})}\cos[m_a(t_n - L_p - \mathbf{v}\cdot\mathbf{x}_p) + \phi_{\mathbf{v}}] - \sqrt{\rho_e f_e(\mathbf{v})}\cos\left(m_a t_n + \phi_{\mathbf{v}}\right)\right\} d^3\mathbf{v}$$

(p denotes light source: L_p is distance to Earth; t_n is signal receiving time; others for ALDM field properties)

A variety of astrophysical light sources proposed before to constrain *g*

- Carroll, Field, Jackiw, PRD 41, 1231 (1990)
- Antonucci, Ann. Rev. Astron. Astrophys. 31, 473 (1993).
- Ivanov, Kovalev, Lister, Panin, Pushkarev, Savolainen, Troitsky, JCAP 02, 059 (2019), 1811.10997
- Fujita, Tazaki, Toma, Phys. Rev. Lett. 122, 191101 (2019), 1811.03525
- Liu, Smoot, Zhao, Phys. Rev. D 101, 063012 (2020), 1901.10981.
- Caputo, Sberna, Frias, Blas, Pani, Shao, Yan, Physical Review D 100, 063515 (2019).
- Chigusa, Moroi, Nakayama, Phys. Lett. B 803, 135288 (2020), 1911.09850.
- Chen, Shu, Xue, Yuan, Zhao, Phys. Rev. Lett. 124, 061102 (2020), 1905.02213
- …

Yet, **spatial correlations of the signal among individual sources** not properly considered

ALDM induced signal for PPAs

- PA rotation signal on PPAs with many pulsars Liu, Lou, **JR**, arXiv: 2111.10615

construct a **signal vector** $\mathbf{s} \equiv (\Delta\theta_{1,1}, ..., \Delta\theta_{1,N_1}, ..., \Delta\theta_{\mathcal{N},1}, ..., \Delta\theta_{\mathcal{N},N_\mathcal{N}})^T$ from the time series of data points for each pulsar in PPA (each point defined by one average polarization profile over some integration time to avoid jitter noise but not ruin ALDM oscillation pattern). Integrating out the random variables, **the signal s follows a multivariable Gaussian distribution with zero mean and the covariance matrix Σ**,

$$\Sigma^{(s)}_{p,n;q,m} \approx \frac{g^2}{m_a^2}\left\{\rho_e \cos(m_a\Delta t) + \sqrt{\rho_p\rho_q}\cos[m_a(\Delta t - \Delta L)]\frac{\sin y_{pq}}{y_{pq}} + ...\right\}$$

p,*q* for a pair of pulsars
n,*m* for data points in time

(*ΔL* relates to time delay; siny/y measures spatial correlation; $y_{pq} = \Delta x/l_c$; $l_c = 1/(m_a v_0)$ is **coherence length**)

ALDM induced signal for PPAs

- PA rotation signal on PPAs with many pulsars Liu, Lou, **JR**, arXiv: 2111.10615

construct a **signal vector** $\mathbf{s} \equiv (\Delta\theta_{1,1}, ..., \Delta\theta_{1,N_1}, ..., \Delta\theta_{\mathcal{N},1}, ..., \Delta\theta_{\mathcal{N},N_\mathcal{N}})^T$ from the time series of data points for each pulsar in PPA (each point defined by one average polarization profile over some integration time to avoid jitter noise but not ruin ALDM oscillation pattern). Integrating out the random variables, **the signal s follows a multivariable Gaussian distribution with zero mean and the covariance matrix Σ**,

$$\Sigma^{(s)}_{p,n;q,m} \approx \frac{g^2}{m_a^2}\left\{\rho_e \cos(m_a \Delta t) + \sqrt{\rho_p \rho_q}\cos[m_a(\Delta t - \Delta L)]\frac{\sin y_{pq}}{y_{pq}} + ...\right\}$$

p,q for a pair of pulsars
n,m for data points in time

(ΔL relates to time delay; siny/y measures spatial correlation; $y_{pq} = \Delta x / l_c$; $l_c = 1/(m_a v_0)$ is **coherence length**)

Comparison	SGWB	ALDM (PTAs and PPAs)
Earth-term correlation	quadrupolar correlation	monopolar correlation (universal)
pulsar-term contribution	pulsar-terms suppressed in $L \gg 1/\omega$ limit, with spatial correlations rapidly degrade	spatial correlations degrade slower ($L \gg l_c \gg 1/m_a$), encode DM density dep., enhanced at galactic center

ALDM motivate incorporating pulsars more broadly distributed in our galaxy in arrays, e.g. the ones near the galactic center

Pulsar correlations

Considering background $\mathbf{n}$ dominated by white noise, data $\mathbf{d} = \mathbf{s} + \mathbf{n}$ follows a multivariate Gaussian distribution with zero mean and covariance matrix $\boldsymbol{\Sigma} = \boldsymbol{\Sigma}^{(s)} + \boldsymbol{\Sigma}^{(n)}$. Likelihood function given the ALDM signal model: $\mathcal{L}(\theta|\mathbf{d}) = \det[2\pi\boldsymbol{\Sigma}]^{-1/2} \exp\left[-\frac{1}{2}\mathbf{d}^T \cdot \boldsymbol{\Sigma}^{-1} \cdot \mathbf{d}\right]$

Exclusion limit on the coupling g set by TS: $q(g, m_a) \equiv 2[\ln \mathcal{L}(\hat{g}, m_a|\mathbf{d}) - \ln \mathcal{L}(g, m_a|\mathbf{d})]$ ($\hat{g}$ maximizes likelihood)

- TS receives contribution from both **auto-correlation** of individual pulsars $(\boldsymbol{\Sigma}^{(s)}_{pp})$ and **cross-correlation** among different pulsars $(\boldsymbol{\Sigma}^{(s)}_{pq}$ with $p \neq q)$
- **Auto-correlation** useful when noise variances known well enough
- **Cross-correlation** highly valuable to distinguish a signal with long-range spatial correlations from uncorrelated noises

Pulsar correlations

Considering background $\mathbf{n}$ dominated by white noise, data $\mathbf{d} = \mathbf{s} + \mathbf{n}$ follows a multivariate Gaussian distribution with zero mean and covariance matrix $\mathbf{\Sigma} = \mathbf{\Sigma}^{(s)} + \mathbf{\Sigma}^{(n)}$. Likelihood function given the ALDM signal model: $\mathcal{L}(\theta|\mathbf{d}) = \det[2\pi\mathbf{\Sigma}]^{-1/2} \exp\left[-\frac{1}{2}\mathbf{d}^T \cdot \mathbf{\Sigma}^{-1} \cdot \mathbf{d}\right]$

Exclusion limit on the coupling g set by TS: $q(g, m_a) \equiv 2[\ln \mathcal{L}(\hat{g}, m_a|\mathbf{d}) - \ln \mathcal{L}(g, m_a|\mathbf{d})]$ ($\hat{g}$ maximizes likelihood)

NANOGrav reported sinusoidal trends of PA rotation with period ~1-2 years

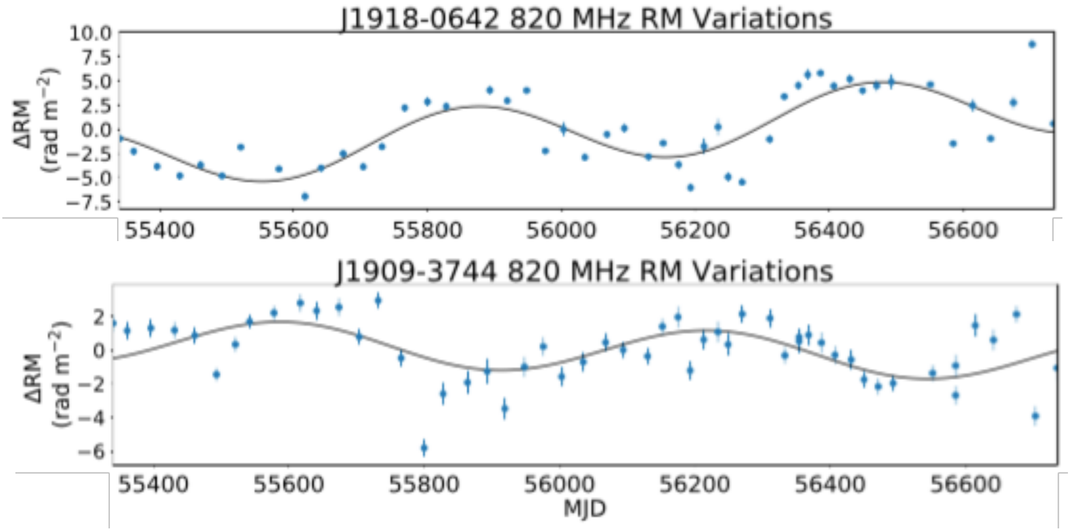

Wahl et al. (NANOGrav), 2104.05723.

auto-corr v.s. cross-corr limits

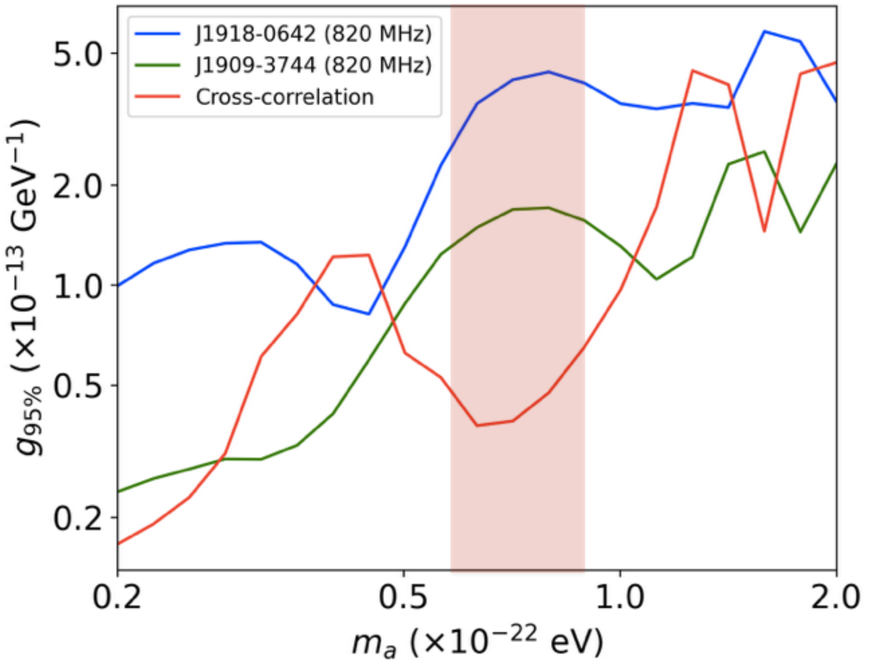

Pulsar correlations

Considering background $\mathbf{n}$ dominated by white noise, data $\mathbf{d} = \mathbf{s} + \mathbf{n}$ follows a multivariate Gaussian distribution with zero mean and covariance matrix $\boldsymbol{\Sigma} = \boldsymbol{\Sigma}^{(s)} + \boldsymbol{\Sigma}^{(n)}$. Likelihood function given the ALDM signal model: $\mathcal{L}(\theta|\mathbf{d}) = \det[2\pi\boldsymbol{\Sigma}]^{-1/2} \exp\left[-\frac{1}{2}\mathbf{d}^T \cdot \boldsymbol{\Sigma}^{-1} \cdot \mathbf{d}\right]$

Asimov TS for projection: $\langle q \rangle \approx \frac{1}{2}\sum_{p,q} \frac{1}{\lambda_p \lambda_q} \mathrm{Tr}\left(\boldsymbol{\Sigma}^{(s)}_{pq}\boldsymbol{\Sigma}^{(s)}_{qp}\right)$ (λ noise variance)

Auto-correlation

$$\mathrm{Tr}\left(\boldsymbol{\Sigma}^{(s)}_{pp}\boldsymbol{\Sigma}^{(s)}_{pp}\right) \sim \frac{g^4}{m_a^4} N_p^2 \left[\rho_e + \rho_p - 2\sqrt{\rho_e \rho_p}\cos(m_a L_p)\right]$$

# of data points for p-th pulsar

$$\frac{\sin y_{ep}}{y_{ep}}\Big]^2 . \quad y_{ep} = L_p/l_c$$

- N_p enhancement reflects temporal correlation, insensitive to distribution of sampled points
- Earth-pulsar correlation (3rd) suppressed if $L_\mathrm{p} \gg l_\mathrm{c}$ or distance uncertainty $\delta L_\mathrm{p} \gg 1/m_\mathrm{a}$

Cross-correlation

$$\mathrm{Tr}\left(\boldsymbol{\Sigma}^{(s)}_{pq}\boldsymbol{\Sigma}^{(s)}_{pq}\right) \sim \frac{g^4}{m_a^4} N_p N_q \left[\rho_e^2 + \rho_p \rho_q \frac{\sin^2 y_{pq}}{y_{pq}^2}\right.$$

$$\left. + 2\rho_e\sqrt{\rho_p \rho_q}\cos(m_a \Delta L)\frac{\sin y_{pq}}{y_{pq}} + f(y_{ep}, y_{eq})\right] .$$

- Earth-terms cross-correlations (1st) universal
- **Pulsar-terms cross-correlations** (2nd) dominate for pulsars around galactic center (separation not too large); suffer less from distance uncertainty

PPA projected sensitivity to ALDM

- Three PPA scenarios (different stage of PTAs)

  NPPA: 100MSPs around 1kpc (*current PTAs*)
  FPPA: 100MSPs in galactic bulge (*FAST/SKA era*)
  OPPA: 1000MSPs following ATNF (*FAST/SKA era*)

- Galactic ALDM density profile: soliton formed by quantum pressure ($r < l_c$, $\rho_c \propto m_a^2$) + NFW ($r > l_c$); CMB constraints on relic abundance imposed

- Pulsar distance uncertainty ~20%, marginalized in constraints estimate

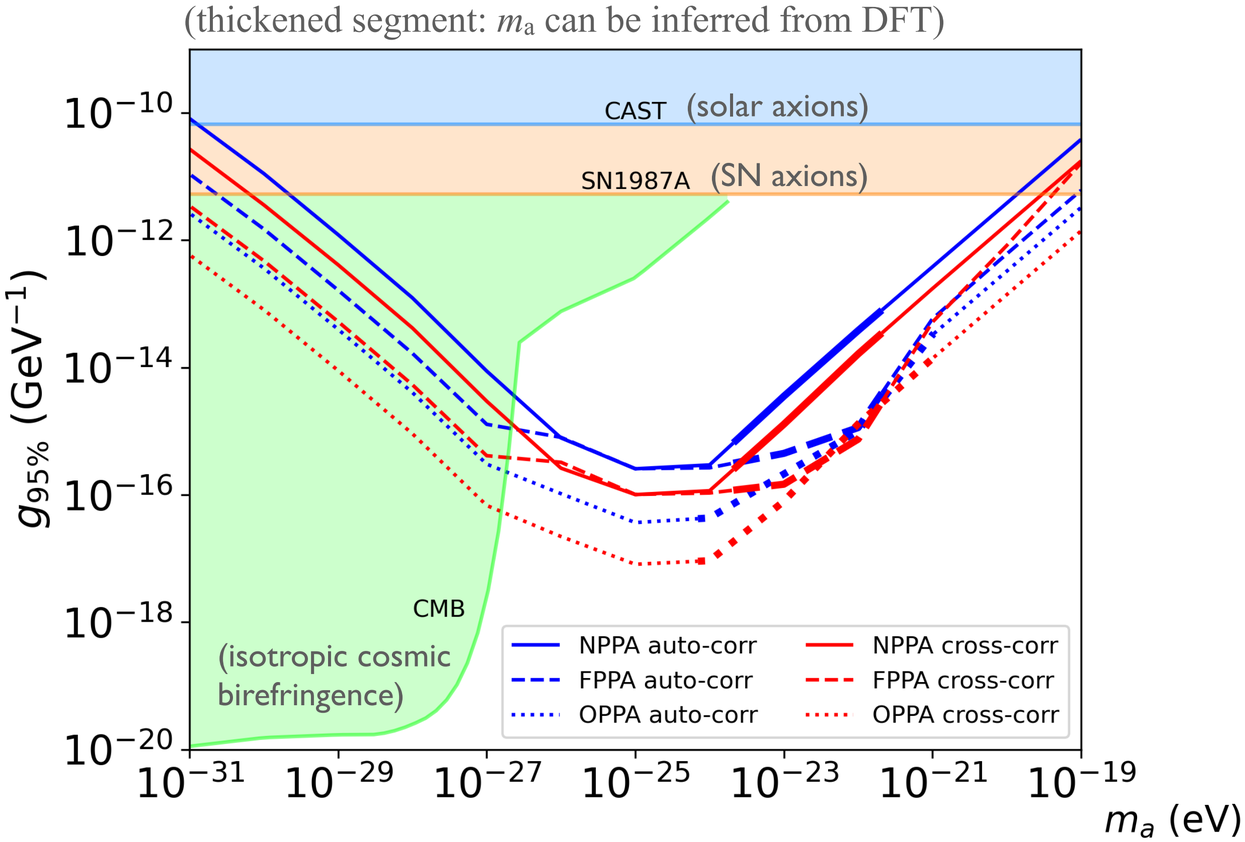

PPA projected sensitivity to ALDM

- Three PPA scenarios (different stage of PTAs)

  NPPA: 100MSPs around 1kpc (*current PTAs*)

  FPPA: 100MSPs in galactic bulge (*FAST/SKA era*)

  OPPA: 1000MSPs following ATNF (*FAST/SKA era*)

- Galactic ALDM density profile: soliton formed by quantum pressure ($r < l_c$, $\rho_c \propto m_a^2$) + NFW ($r > l_c$); CMB constraints on relic abundance imposed

- Pulsar distance uncertainty ~20%, marginalized in constraints estimate

- Cross-correlation limits typically stronger than auto-correlation ones. As m_a decreases, the limit (1) decrease; (2) stay approx. flat; (3) increase

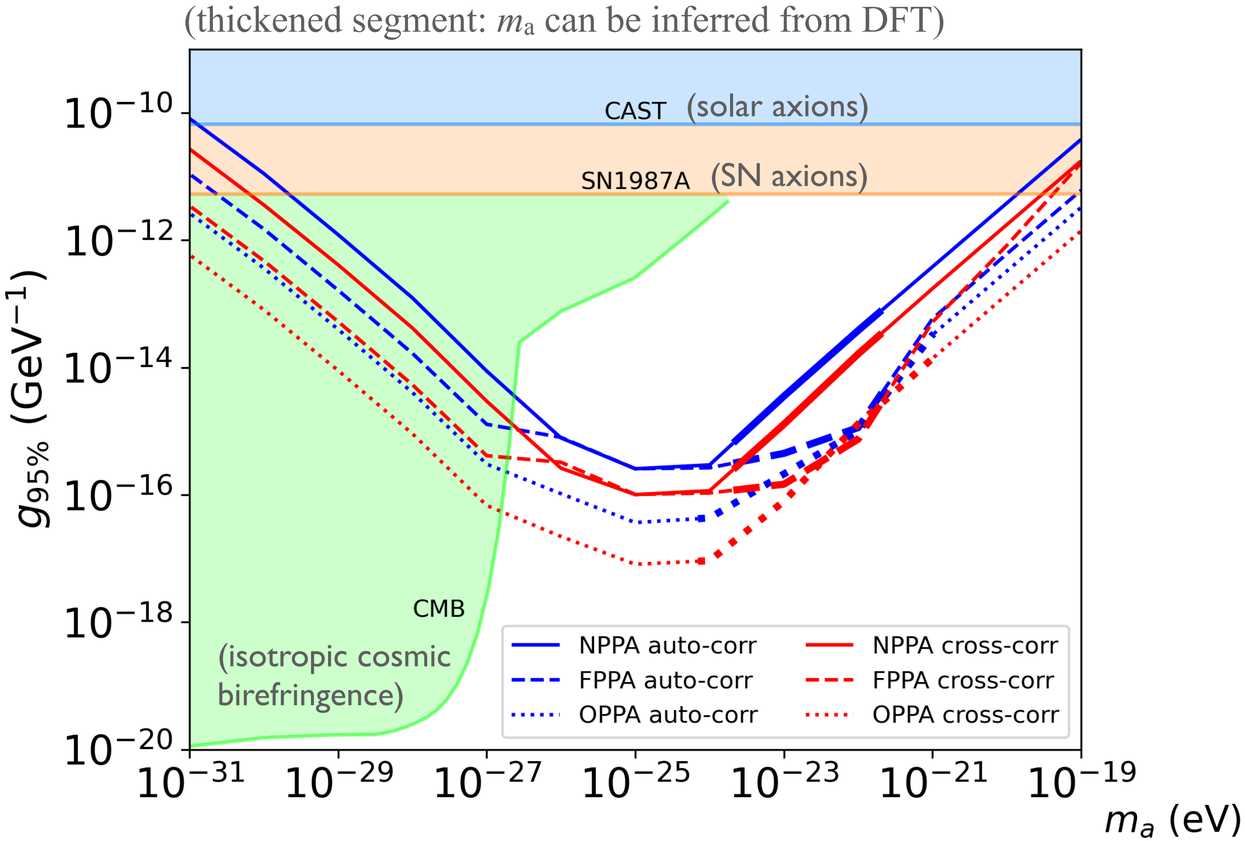

PPA projected sensitivity to ALDM

- Three PPA scenarios (different stage of PTAs)

  NPPA: 100MSPs around 1kpc (*current PTAs*)
  FPPA: 100MSPs in galactic bulge (*FAST/SKA era*)
  OPPA: 1000MSPs following ATNF (*FAST/SKA era*)

- Galactic ALDM density profile: soliton formed by quantum pressure ($r < l_c$, $\rho_c \propto m_a^2$) + NFW ($r > l_c$); CMB constraints on relic abundance imposed

- Pulsar distance uncertainty ~20%, marginalized in constraints estimate

- Cross-correlation limits typically stronger than auto-correlation ones. As m_a decreases, the limit (1) decrease; (2) stay approx. flat; (3) increase

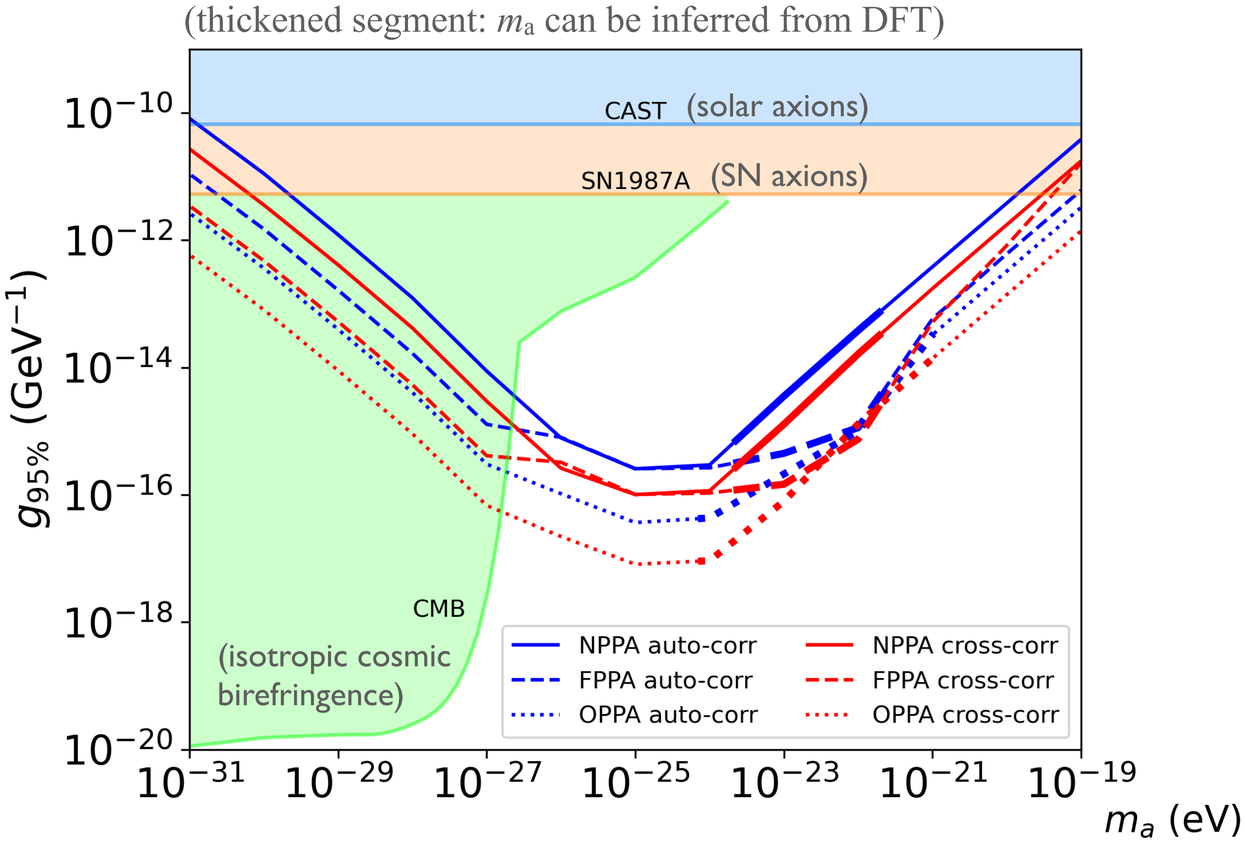

NPPA: (1) auto-corr limit ~ $m_a\,\lambda^{1/2}N_p^{-1/2}\rho_e^{-1/2}\mathcal{N}^{-1/4}$; cross-corr improved by $\mathcal{N}^{-1/4}$; (2) m_a dep. cancels as pulsars in soliton core; (3) Earth-pulsar terms yield large cancellation

PPA projected sensitivity to ALDM

- Three PPA scenarios (different stage of PTAs)

  NPPA: 100MSPs around 1kpc (*current PTAs*)
  FPPA: 100MSPs in galactic bulge (*FAST/SKA era*)
  OPPA: 1000MSPs following ATNF (*FAST/SKA era*)

- Galactic ALDM density profile: soliton formed by quantum pressure ($r < l_c$, $\rho_c \propto m_a^2$) + NFW ($r > l_c$); CMB constraints on relic abundance imposed

- Pulsar distance uncertainty ~20%, marginalized in constraints estimate

- Cross-correlation limits typically stronger than auto-correlation ones. As m_a decreases, the limit (1) decrease; (2) stay approx. flat; (3) increase

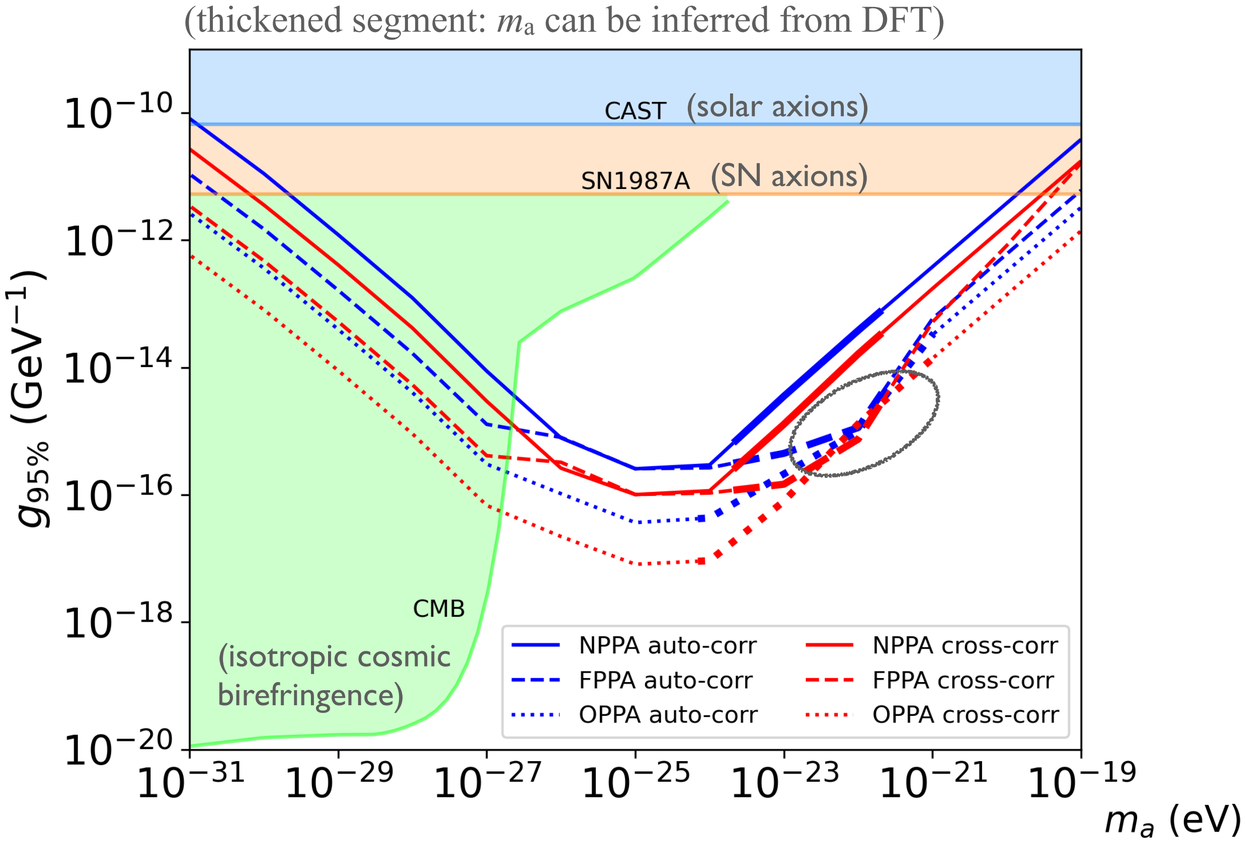

FPPA benefits from soliton enhanced density, best for fuzzy DM with $\rho_p/\rho_e \sim 10^5$; while cross-correlation limit degrades for larger m_a due to small l_c

PPA projected sensitivity to ALDM

- Three PPA scenarios (different stage of PTAs)

  NPPA: 100MSPs around 1kpc (*current PTAs*)

  FPPA: 100MSPs in galactic bulge (*FAST/SKA era*)

  OPPA: 1000MSPs following ATNF (*FAST/SKA era*)

- Galactic ALDM density profile: soliton formed by quantum pressure ($r < l_c$, $\rho_c \propto m_a^2$) + NFW ($r > l_c$); CMB constraints on relic abundance imposed

- Pulsar distance uncertainty ~20%, marginalized in constraints estimate

- Cross-correlation limits typically stronger than auto-correlation ones. As m_a decreases, the limit (1) decrease; (2) stay approx. flat; (3) increase

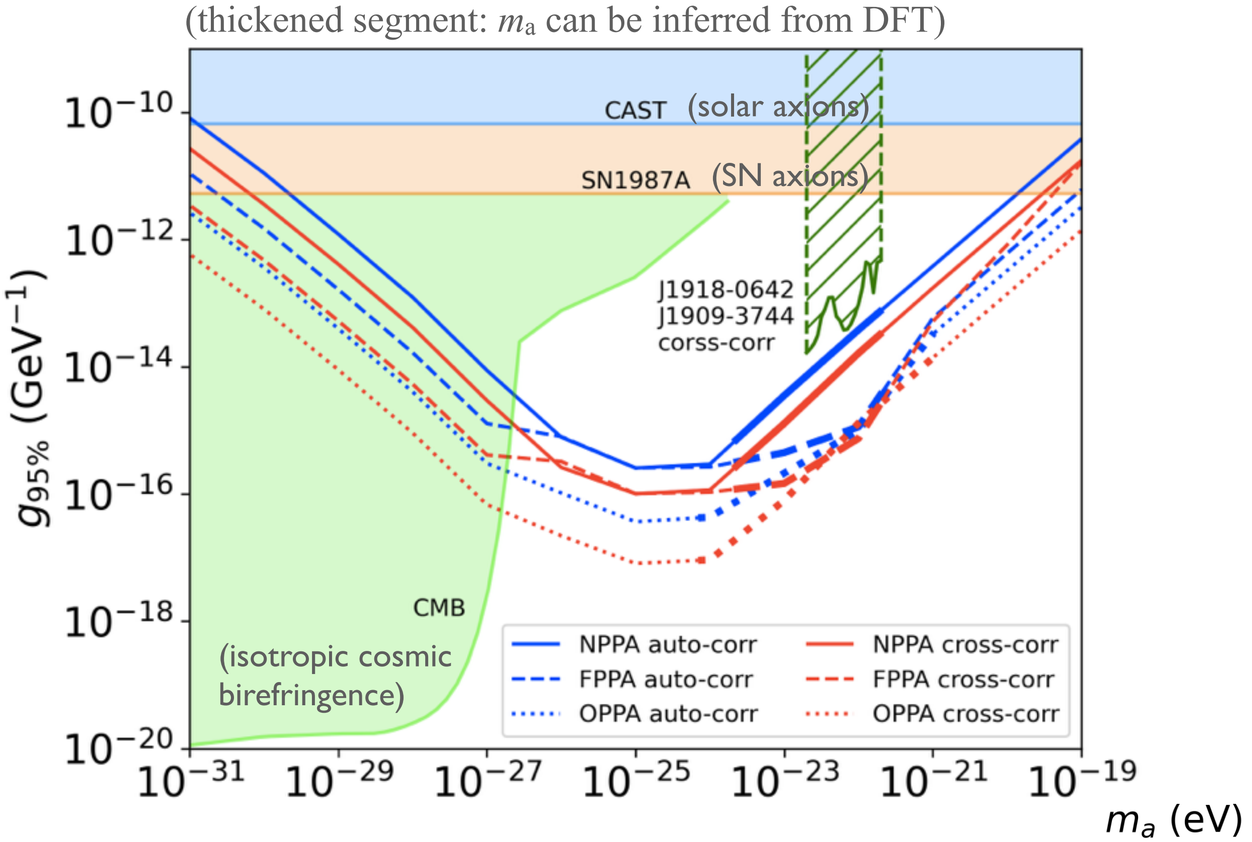

Preliminary limits from cross-correlation of PA rotation of two MSPs from NANOGrav. Complementary to the existing bounds.

Summary and Outlook

- We propose the development of PPAs with the same data acquired for PTAs, which take up a significant amount of resources of radio telescope
- Considering ultralight ALDM as an example, PPAs can be used to detect cosmic birefringence induced by its Chern-Simon coupling. The projected PPA limits form a great complementarity with existing bounds
- Cross-correlation of oscillating signals on PPAs and PTAs can further strengthen the ALDM detectability
- More physical targets for PPAs as a new tool for exploring fundamental physics?
- Synergize PPAs with other observations (e.g. CMB polarization) to improve the capability to distinguish different scenarios

Thank You!

More for PPA projected sensitivity

✦ **Three PPA scenarios (different stage of PTAs)**

- **Near PPA (NPPA)**: 100 MSPs around the Earth (we take observed MSPs in the ATNF Pulsar Catalogue with $0.50\text{kpc} \leq L_p \leq 1.52\text{kpc}$). Each pulsar has $N_p = 100$ data points with a constant time separation over $T_p = 10$ years. The noise variance $\lambda = (1\text{deg})^2$, typical for the current PA measurements from PTAs

- **Far PPA (FPPA)**: 100 MSPs randomly but uniformly distributed within a (1.0 kpc) cube around galactic center, i.e, the bulge area. N_p, T_p and λ for each pulsar are assumed the same as NPPA

- **Optimal PPA (OPPA)**: 1000 MSPs randomly distributed following MSP data in the ATNF Pulsar Catalogue. As a more aggressive choice of parameters for each pulsar, we assume $T_p = 30$ year, with an observational cadence of 1/(one week) and hence $N_p \approx 1500$ data points. λ is the same as NPPA.

✦ **More about noise:** radiometer noise dominates for fainter pulsars with a small SNR, while the jitter noise limits the sensitivity of bright pulsars. If jitter noise dominates (most likely in FAST/SKA era), the sensitivity can be strongly constrained by the available telescope resources.

Galactic ALDM density profile

In the absence of full simulation for the overall profile of halo with various m_a values and relic-abundance shares in DM remains in literatures, we consider simple profile: **cored soliton + NFW profile + CMB constraints on relic abundance**

$$\rho(r) = \kappa \times \begin{cases} \frac{0.019(\frac{m_a}{m_{a,0}})^{-2}(\frac{r_c}{1\mathrm{kpc}})^{-4}}{[1+9.1\times10^{-2}(\frac{r}{r_c})^2]^8} M_\odot \mathrm{pc}^{-3}, & \text{for } r < l_c. \\ \frac{\rho_0}{r/R_H(1+r/R_H)^2}, & \text{for } r > l_c \ . \end{cases}$$

$$r_c \approx 100\mathrm{pc} \times m_{a,0}/m_a$$

- Cored soliton-like structure found from simulation of fuzzy DM, with r_c obtained by fitting to the observed DM density at galactic center [Schive, Chiueh, and Broadhurst, Nature Phys. 10, 496 (2014)]
- NFW parameters normalized with the local DM density near the Earth; the two profiles smoothened with hyperbolic tangent function at r~l_c
- ALDM relic abundance $\varkappa$ constrained by CMB anisotropies [Marsh, Phys. Rept. 643, 1 (2016)]

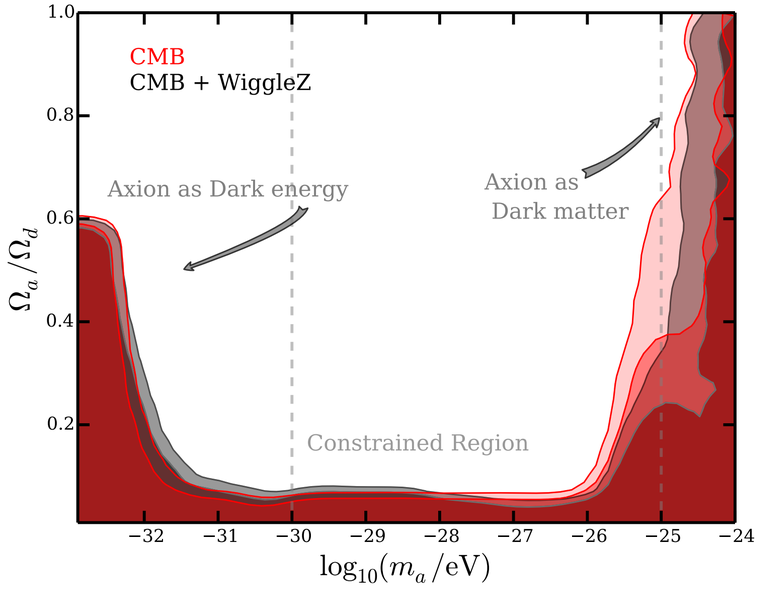

More on pulsar temporal correlations

Auto-correlation

The contribution decomposed as

$$\mathbf{\Sigma}^{(s)}_{pp} \approx A_{pp}\hat{\mathbf{\Sigma}}^{(s)}_{pp}\,.$$

temporal correlation encoded in the matrix

$$\hat{\Sigma}^{(s)}_{p,n;p,m} \;=\; \cos[m_a(t_{p,n} \;-\; t_{p,m})]$$

- Ideal case N_p data points sampled uniformly with constant separation p

$$\mathrm{Tr}\left(\hat{\mathbf{\Sigma}}^{(s)}_{pp}\hat{\mathbf{\Sigma}}^{(s)}_{pp}\right) = \frac{1}{2}\left[N_p^2 + \left(\frac{\sin(m_a T_p)}{\sin(m_a\tau_p)}\right)^2\right]$$

- Random sampling, bounded from below by $N_p{}^2/2$

$$\frac{\mathrm{Tr}(\hat{\mathbf{\Sigma}}^{(s)}_{pp}\hat{\mathbf{\Sigma}}^{(s)}_{pp})}{(N_p^2/2)} - 1 \propto \frac{1}{N_p}\frac{1}{m_a T_p}$$

constraint not very sensitive to the data-taking strategy

Cross-correlation

The contribution decomposed as

$$\mathbf{\Sigma}^{(s)}_{pq} \approx A_{pq}\,\hat{\mathbf{\Sigma}}^{(s)}_{pq} + A'_{pq}\,\hat{\mathbf{\Sigma}}'^{(s)}_{pq}$$

temporal correlation encoded in two matrixes

$$\hat{\Sigma}'^{(s)}_{p,n;q,m} = \sin[m_a(t_{p,n} - t_{q,m})]$$

- Ideal case of uniform sampling

$$\mathrm{Tr}\left(\mathbf{\Sigma}^{(s)}_{pq}\mathbf{\Sigma}^{(s)}_{pq}\right) = \frac{1}{2}(A^2_{pq} + A'^2_{pq})N_pN_q$$
$$+\frac{1}{2}(A^2_{pq} - A'^2_{pq})\frac{\sin(m_aT_p)}{\sin(m_a\tau_p)}\frac{\sin(m_aT_q)}{\sin(m_a\tau_q)}\cos\Theta$$
$$+A_{pq}A'_{pq}\frac{\sin(m_aT_p)}{\sin(m_a\tau_p)}\frac{\sin(m_aT_q)}{\sin(m_a\tau_q)}\sin\Theta\,.$$
$$\Theta = m_a(t_{p,N_p} - t_{q,N_q} + t_{p,1} - t_{q,1})$$

- Random sampling, $\mathrm{Tr}(\hat{\mathbf{\Sigma}}^{(s)}_{pq}\hat{\mathbf{\Sigma}}^{(s)}_{pq}) - N_pN_q/2$, $\mathrm{Tr}(\hat{\mathbf{\Sigma}}'^{(s)}_{pq}\hat{\mathbf{\Sigma}}'^{(s)}_{pq}) - N_pN_q/2$ and $\mathrm{Tr}(\hat{\mathbf{\Sigma}}^{(s)}_{pq}\hat{\mathbf{\Sigma}}'^{(s)}_{pq})$ follow narrow distribution around zero